Temperature-Sensitivity of Two Microwave HEMT Devices: AlGaAs/GaAs vs. AlGaN/GaN Heterostructures

Mohammad Abdul Alim [1] , Abu Zahed Chowdhury [1], Shariful Islam [1], Christophe Gaquiere [2] and Giovanni Crupi [3,*]

1   Department of Electrical and Electronic Engineering, University of Chittagong, Chittagong 4331, Bangladesh; mohammadabdulalim@cu.ac.bd (M.A.A.); zahed_apece@cu.ac.bd (A.Z.C.); shariful2488@cu.ac.bd (S.I.)
2   Institute of Electronic, Microelectronic and Nanotechnology (IEMN), The University of Lille, F-59000 Lille, France; christophe.gaquiere@iemn.univ-lille1.fr
3   Department of Biomedical and Dental Sciences and Morphofunctional Imaging, University of Messina, 98125 Messina, Italy
*   Correspondence: crupig@unime.it

Abstract: The goal of this paper is to provide a comparative analysis of the thermal impact on the microwave performance of high electron-mobility transistors (HEMTs) based on GaAs and GaN technologies. To accomplish this challenging goal, the relative sensitivity of the microwave performance to changes in the ambient temperature is determined by using scattering parameter measurements and the corresponding equivalent-circuit models. The studied devices are two HEMTs with the same gate width of 200 μm but fabricated using different semiconductor materials: GaAs and GaN technologies. The investigation is performed under both cooled and heated conditions, by varying the temperature from −40 °C to 150 °C. Although the impact of the temperature strongly depends on the selected operating condition, the bias point is chosen in order to enable, as much as possible, a fair comparison between the two different technologies. As will be shown, quite similar trends are observed for the two different technologies, but the impact of the temperature is more pronounced in the GaN device.

Keywords: GaAs; GaN; heterostructure; high electron-mobility transistor (HEMT); microwave performance; temperature-sensitivity

1. Introduction

High electron-mobility transistors (HEMTs, also known as a heterostructure or heterojunction FETs) based on AlGaAs/GaAs and AlGaN/GaN heterostructures have greatly evolved since their inception in the early 1980s [1] and early 1990s [2], respectively. The most evident difference between the GaAs and GaN technologies is that the former is more mature, whereas the latter is more suited for high-power applications, owing to its wide bandgap nature. Over the years, many studies have focused on the high-frequency characterization and modeling of the temperature-dependent behavior of both GaAs [3–12] and GaN [13–27] HEMTs. This is because the operating temperature can remarkably affect the device performance, reliability, and lifetime, which are key features in practical applications, especially those in harsh environmental conditions [28]. With the aim of contributing to the assessment of the impact of the temperature on GaAs and GaN technologies, this article presents a comparative investigation of the temperature-dependent high-frequency behavior of two HEMTs based on AlGaAs/GaAs and AlGaN/GaN heterojunctions. To enable this comparative investigation, a sensitivity-based analysis is developed. The assessment of the sensitivity of the two HEMTs to changes in the ambient temperature (T_a) has been accomplished by using equivalent circuit models extracted from scattering (*S-*) parameters. The ambient temperature has been swept over a wide range of values, going from −40 °C to 150 °C. The bias point has been selected in order to allow, as much as

possible, a fair comparison between the two different transistor technologies. The GaAs and GaN HEMTs have the same gate width of 200 μm but differ in the gate lengths, which are 0.25 μm and 0.5 μm, respectively. For the first time, the challenging task of comparing the temperature-dependent performance of the two different semiconductor technologies is accomplished by reporting an extensive and systematic sensitivity-based analysis, which is carried out by using the drain current (I_{ds}), the equivalent-circuit parameters (ECPs), and the major RF figures of merit. The degradations of the device performance at a higher T_a are found to be more pronounced for the GaN technology, which can be attributed to the higher dissipated power (P_{diss}). It is worth noting that the two tested technologies are inherently different and that this then clearly impacts on the achieved results. Given the widely different characteristics of the two tested technologies, it is really not feasible to distinguish each contribution arising from the different operating conditions (e.g., dissipated power) and peculiar device physics (e.g., thickness and thermal conductivity of the substrate). Hence, the reported comparative analysis has not aimed at distinguishing each contribution but at assessing the overall impact of the ambient temperature on the DC and microwave characteristics of the two tested technologies. Nevertheless, for the sake of completeness, it should be underlined that the channel temperature is higher than the ambient temperature because of the heat generated by the self-heating effects, which are strongly dependent not only on the dissipated power level but also on the thickness and thermal conductivity of the materials [13,29–36]. Furthermore, it is worth mentioning that the extraction of the equivalent-circuit elements may be inevitable affected by the uncertainty inherent in measurements and that, in addition, the model topology itself is an approximation of the device physics [37–43], which in turn may impact on the achieved temperature-dependent findings.

The remainder of this article is organized as follows: Section 2 is focused on the description of the tested device and experiments, Section 3 is devoted to the sensitivity-based analysis and the discussion of the findings, and the last section summarizes the main conclusions of this study.

2. Devices and Experiments

The two studied devices are an AlGaAs/GaAs HEMT grown by molecular beam epitaxy (MBE) on a semi-insulating undoped GaAs substrate and an AlGaN/GaN HEMT grown by metal-organic chemical vapor deposition (MOCVD) on a SiC substrate. Figure 1 shows the schematic cross-sectional views and photos of the two tested HEMTs. The interdigitated layout of both devices is based on the connection in parallel of two fingers, each being 100-μm long, yielding to a total gate width of 200 μm. The gate lengths of the GaAs and GaN devices are 0.25 μm and 0.5 μm, respectively. The source-to-gate distance (L_{SG}) and the gate-to-drain distance (L_{GD}) are 0.5 μm and 2.0 μm for the GaAs device, while their values are equal to 1 μm and 2.75 μm for the GaN device.

The microwave experiment consists of S-parameters measured from 45 MHz to 50 GHz at nine different ambient temperatures: $-40\,°C$, $-25\,°C$, $0\,°C$, $25\,°C$, $50\,°C$, $75\,°C$, $100\,°C$, $125\,°C$, and $150\,°C$. The S-parameters were measured with a vector network analyzer (VNA HP8510C) in conjunction with a DC source (HP4142B) for biasing, a temperature control unit (Temptronic TP03200, Temptronic Corporation, Mansfield, MA, USA) for setting the ambient temperature, and a PC with a specialized software (IC-CAP) for controlling the full measurement procedure through the GPIB interface. The off-wafer calibration was performed using line-reflect-reflect-match (LRRM) standards on the alumina calibration substrate from Cascade Microtech and a commercial calibration software (WinCal). The comparative analysis is performed using S-parameters at the following two bias points in the saturation region: $V_{ds} = 3$ V and $V_{gs} = -0.1$ V for the GaAs HEMT and $V_{ds} = 9$ V and $V_{gs} = -4$ V for the GaN HEMT. This choice has been made based on the analysis of the DC output characteristics of the two transistors at different T_a (see Figures 2 and 3), in order to enable, as much as possible, a fair comparison between the two different technologies. For the GaAs HEMT, two temperature-dependent effects contribute in opposite ways to

the resultant behavior of I_{ds} with an increasing temperature: the degradation of the carrier transport properties and the threshold voltage (V_{th}) shift towards more negative values. Therefore, V_{gs} is selected at -0.1 V, in order to minimize the contribution of the V_{th} shift that plays a more dominant role at lower V_{gs}. V_{ds} is selected at 3 V, in order to avoid the pronounced positive slope of I_{ds} at high V_{ds}. For the GaN HEMT, the temperature-dependent behavior of I_{ds} is mostly due to the degradation of the carrier transport properties and/or to a reduction in the carrier concentration in the two-dimensional electron gas (2DEG). Therefore, V_{ds} and V_{gs} are, respectively, selected at 9 V and -4 V, in order to avoid the pronounced negative slope of I_{ds} (V_{ds}) at a high P_{diss}.
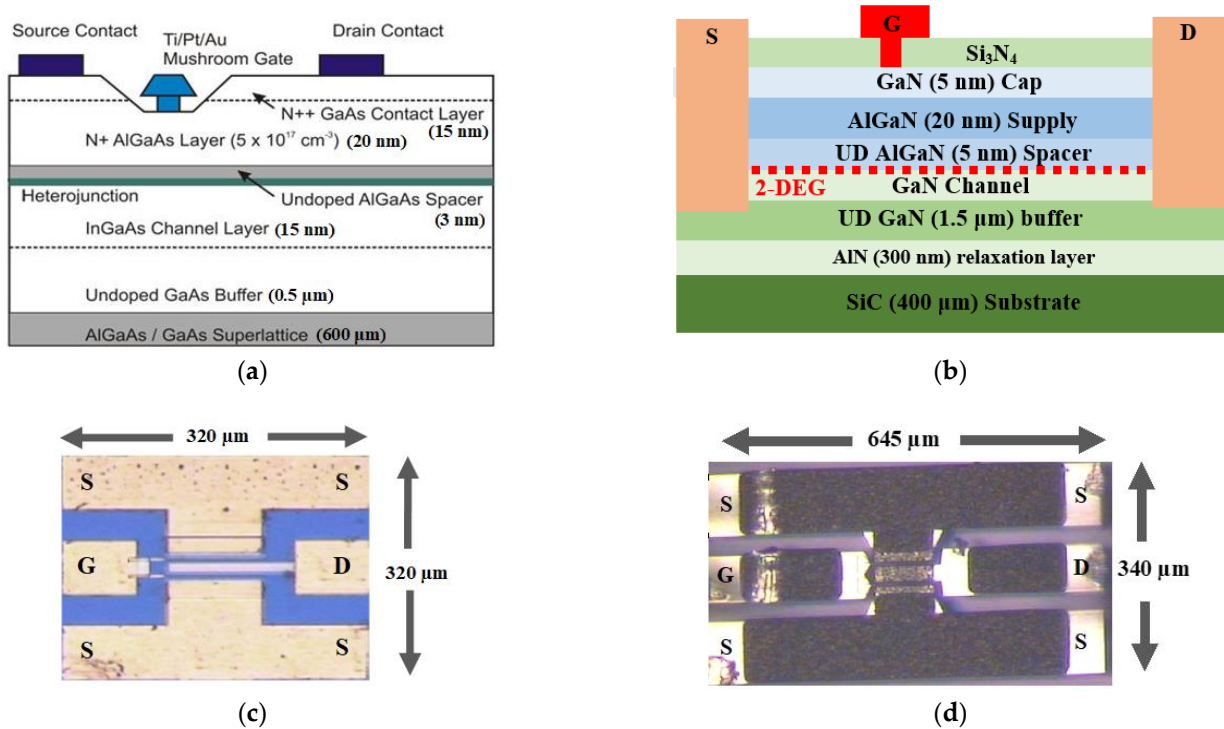

Figure 1. Schematic cross-sectional views and photos of the tested high electron-mobility transistors (HEMTs) based on (**a**,**c**) AlGaAs/GaAs and (**b**,**d**) AlGaN/GaN heterostructures.
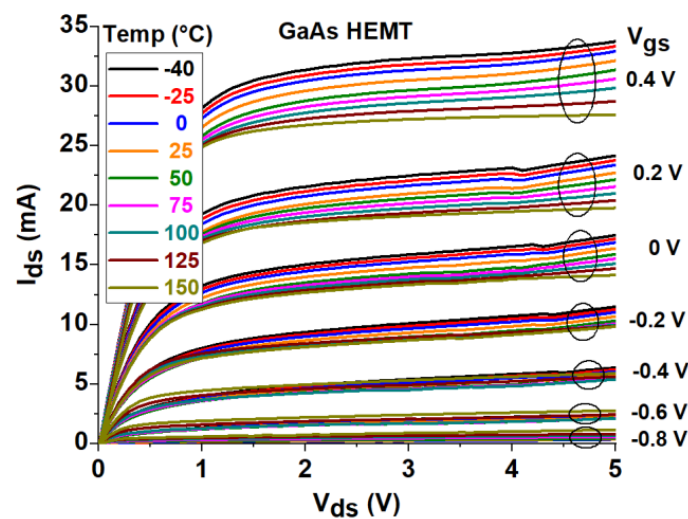

Figure 2. DC output characteristics of the studied GaAs HEMT at different T_a.
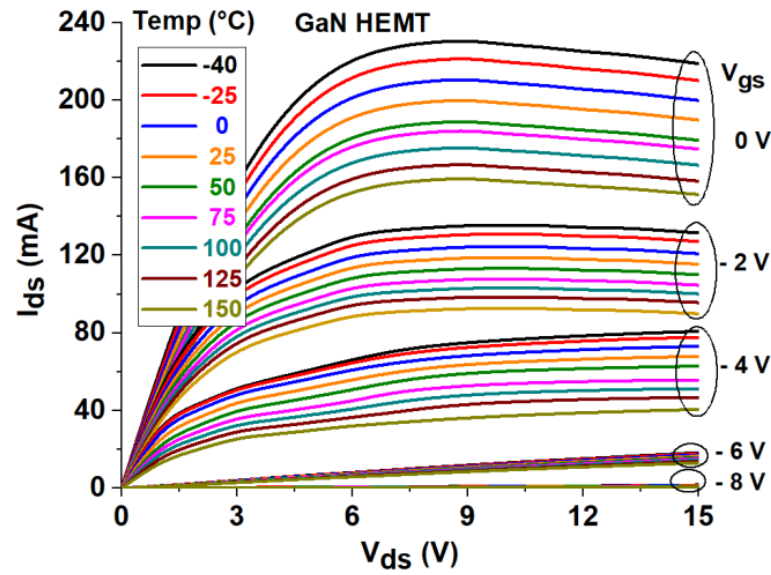
Figure 3. DC output characteristics of the studied GaN HEMT at different T_a.

At the selected bias voltages (see Figure 4), the dimensionless relative sensitivity of I_{ds} with respect to T_a is calculated by normalizing the relative change in I_{ds} to the relative change in T_a:

$$RSI_{ds} = \frac{\Delta I_{ds}}{I_{ds0}} \frac{T_{a0}}{\Delta T_a} = \frac{(I_{ds} - I_{ds0})}{I_{ds0}} \frac{T_{a0}}{(T_a - T_{a0})} \tag{1}$$

where I_{ds0} is the value of I_{ds} at the reference temperature (T_{a0}) of 25 °C. As can be observed in Figure 4, RSI_{ds} is negative for both devices, as a consequence of the fact that an increase in T_a leads to a decrease in I_{ds}, and is of greater magnitude for the GaN technology, as a consequence of the much higher P_{diss} leading to a higher channel temperature (i.e., $T_{ch} = T_a + R_{th}P_{diss}$ where R_{th} is the thermal resistance).
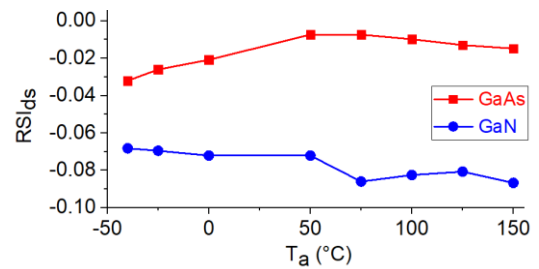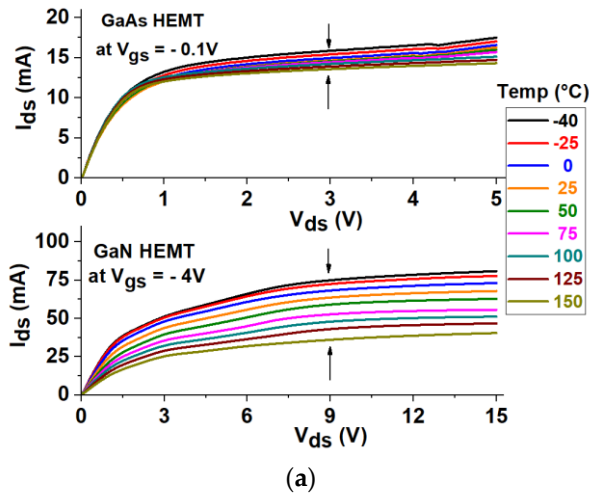

(**a**)

(**b**)

Figure 4. (**a**) The selected bias points for the sensitivity-based analysis are $V_{ds} = 3$ V and $V_{gs} = -0.1$ V for the GaAs HEMT (top plot) and $V_{ds} = 9$ V and $V_{gs} = -4$ V for the GaN HEMT (bottom plot); (**b**) Behavior of RSI_{ds} versus T_a for the studied (red line) GaAs and (blue line) GaN HEMTs.

For the sake of completeness, we report the impact of the ambient temperature on the I_{ds}-V_{gs} curves and the corresponding transconductance at $V_{ds} = 3$ V for the GaAs device and at $V_{ds} = 9$ V for the GaN device (see Figure 5). By increasing the temperature, the drain current and the transconductance are remarkably reduced for the GaN device, whereas

operating bias points at which their values are temperature insensitive (the so-called current and transconductance zero temperature coefficient (CZTC and GZTC) points) can be observed for the GaAs device, owing to the counterbalancing of temperature-dependent effects contributing in opposite ways [12].
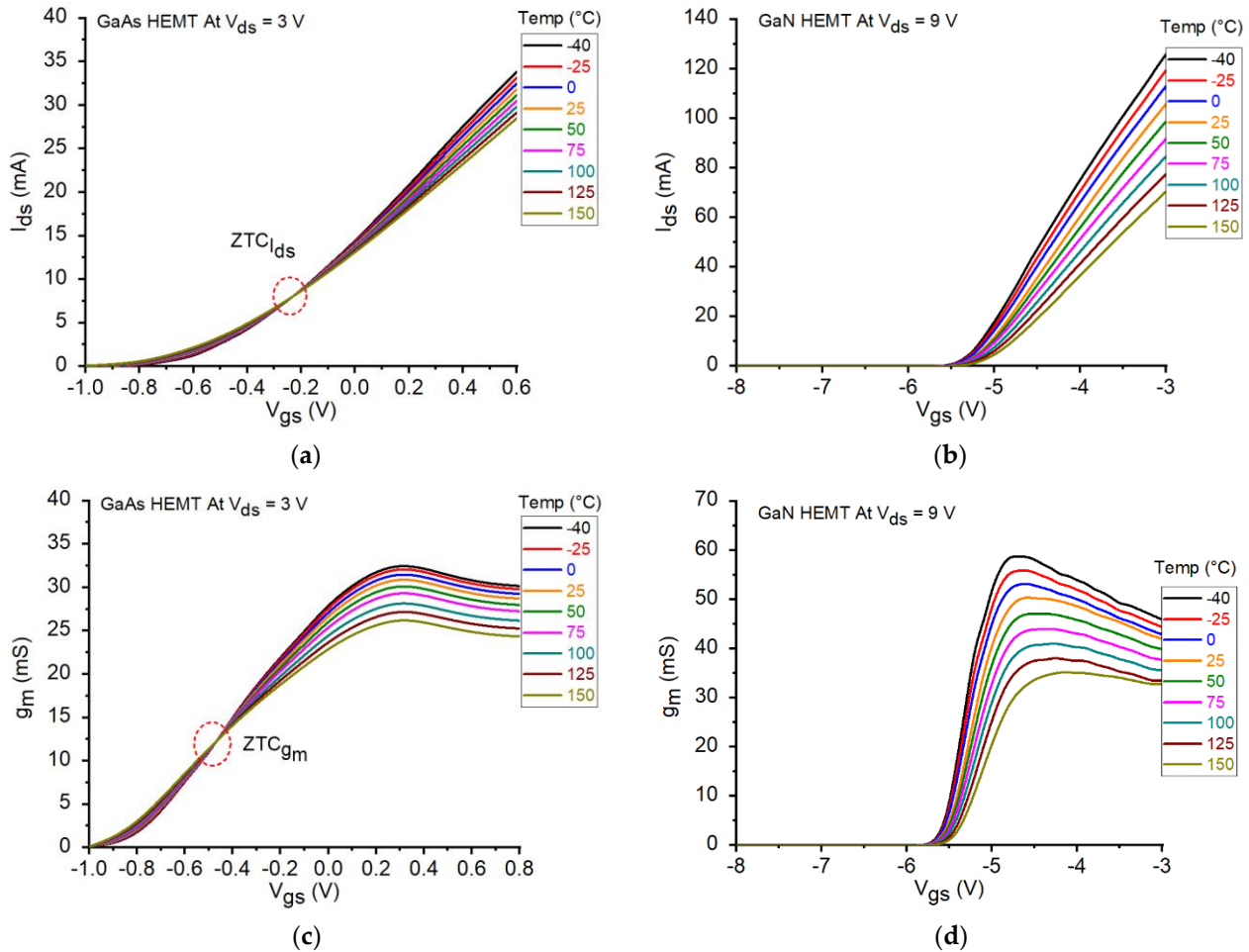

Figure 5. DC transcharacteristics and transconductances at different T_a for (**a**,**c**) the GaAs HEMT at V_{ds} = 3 V and (**b**,**d**) the GaN HEMT at V_{ds} = 9 V.

Figure 6 shows the impact of T_a on the measured *S*-parameters at the selected bias points. By increasing T_a, the low-frequency S_{21} is reduced, due to the degradation of the carrier transport properties. Both devices are affected by the kink effect in S_{22} [44–49], which is more marked at a lower T_a because of the higher g_m. As a matter of fact, it has been demonstrated that the kink effect is mainly due to high values of g_m.
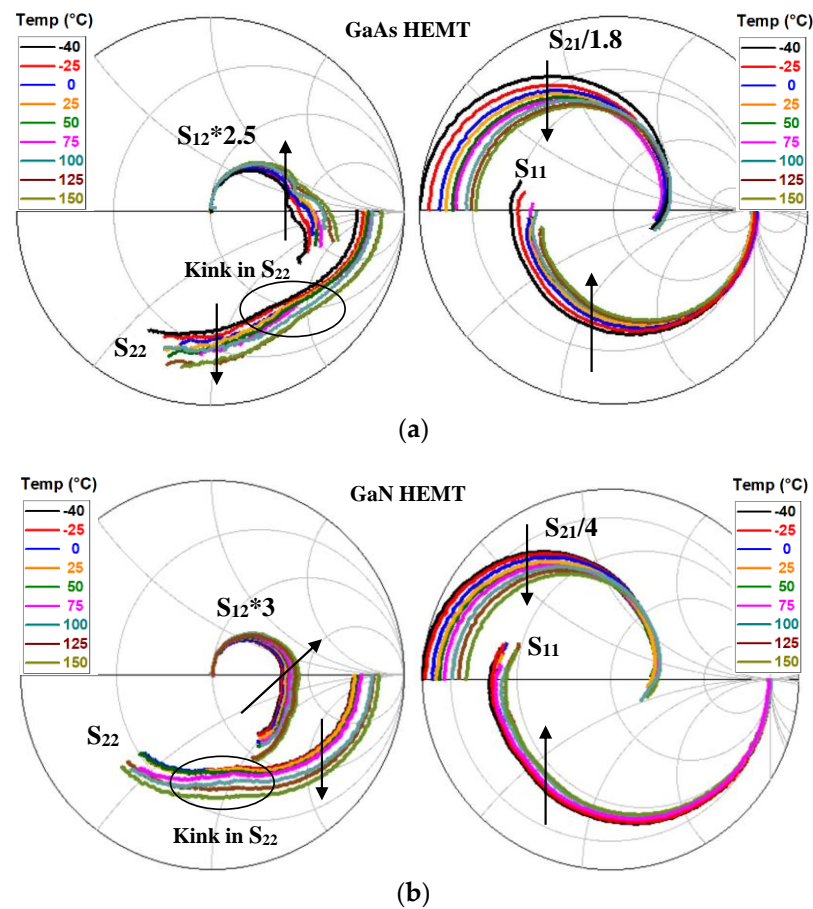
Figure 6. Measured *S*-parameters of the studied (**a**) GaAs and (**b**) GaN HEMTs at different T_a. The illustrated bias points are: $V_{ds} = 3$ V and $V_{gs} = -0.1$ V for the GaAs HEMT and $V_{ds} = 9$ V and $V_{gs} = -4$ V for the GaN HEMT. The frequency range goes from 45 MHz to 50 GHz. ("*" means product (the multiplication operation)).

3. Sensitivity-Based Analysis

The *S*-parameters have been modelled using the equivalent-circuit model in Figure 7. The ECPs have been obtained by using a standard "cold" pinch-off approach [50]. As illustrated in Figure 8, a good agreement between the measured and simulated *S*-parameter has been achieved for the two tested devices.
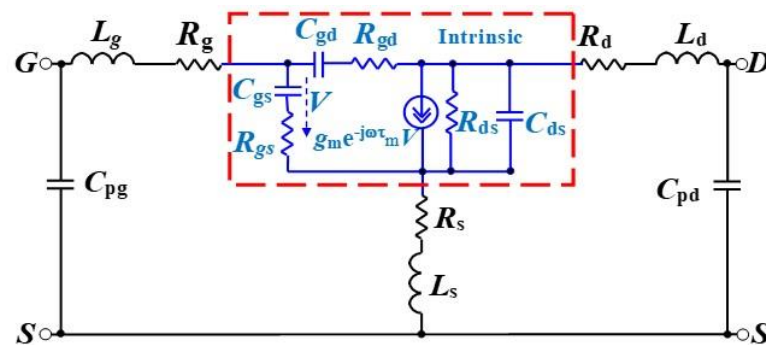

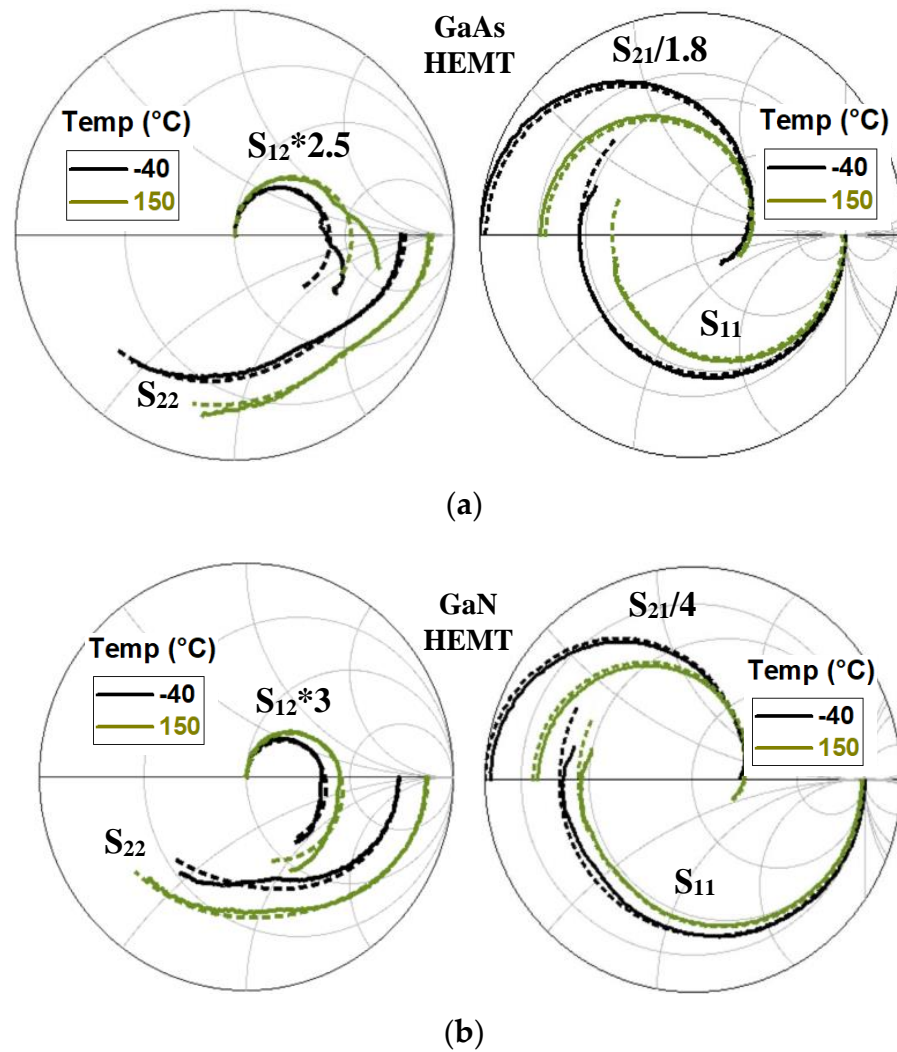**Figure 7.** Equivalent-circuit model for the studied GaAs and GaN HEMTs.

Figure 8. Measured *S*-parameters of the studied (**a**) GaAs and (**b**) GaN HEMTs at different T_a. The illustrated bias points are: V_{ds} = 3 V and V_{gs} = −0.1 V for the GaAs HEMT and V_{ds} = 9 V and V_{gs} = −4 V for the GaN HEMT. The frequency range goes from 45 MHz to 50 GHz. ("*" means product (the multiplication operation)).

Table 1 reports the values of the drain current, the ECPs, the intrinsic input and feedback time constants (i.e., $\tau_{gs} = R_{gs}C_{gs}$ and $\tau_{gd} = R_{gd}C_{gd}$), the unity current gain cut-off frequency (f_t), and the maximum frequency of oscillation (f_{max}). The three intrinsic time constants (τ_m, τ_{gs}, and τ_{gd}) model the intrinsic non-quasi-static (NQS) effects, which arise from the inertia of the intrinsic device in responding to rapid signal changes [51]. The values of f_t and f_{max} are, respectively, determined from the measured short-circuit current gain (h_{21}) and maximum stable/available gain (MSG/MAG). Although the GaAs HEMT has a shorter gate length that should result in a higher operation frequency, the GaN HEMT has smaller time constants (except for τ_{gd}) and higher f_t and f_{max}, which are desired in order to enable device applications at high frequencies. This is can be linked to the fact that the conventional scaling rules cannot be directly applied to make a straightforward comparison between devices that are based on different semiconductor materials, technologies, and layouts. As a matter of fact, this could be foreseen from the values of I_{ds}, which are larger for the GaN HEMT, even if the GaAs HEMT has a shorter gate length that should result in a higher I_{ds}. The same observation can be made for the intrinsic g_m.

Likewise, in the case of I_{ds}, the relative sensitivities of the other parameters in Table 1 are estimated by using Equation (1) and are then illustrated in Figures 9–11. Relative

sensitivities of the extrinsic capacitances and inductances of close to zero were achieved (see Figure 9a–e), owing to their weak temperature dependence. On the other hand, the relative sensitivities of the extrinsic and intrinsic resistances are positive (see Figures 9f–h and 10d–f), due to the increase of the resistive contributions with an increasing T_a. Contrary to the resistances, the transconductance shows a relative sensitivity that is negative (see Figure 11a), enlightening its degradation with an increasing T_a. The relative sensitivities of the intrinsic capacitances can be positive or negative (see Figure 10a–c), depending on the considered device and capacitance. The relative sensitivities of the intrinsic time constants are positive (see Figure 11b–d), reflecting their increase at a higher T_a and thus a shift of the onset of the NQS effects at lower frequencies. On the other hand, the relative sensitivities of the frequencies f_t and f_{max} are negative (see Figure 11e,f), reflecting their decrease at a higher T_a and thus a reduction of the device operation frequencies. The analysis of the relative sensitivities of the crucial parameters such as g_m, f_t, and f_{max} shows that larger negative values are observed for the GaN device compared to the GaAs counterpart (see Figure 11a,e,f), in line with what was seen for I_{ds} (see Figure 4).
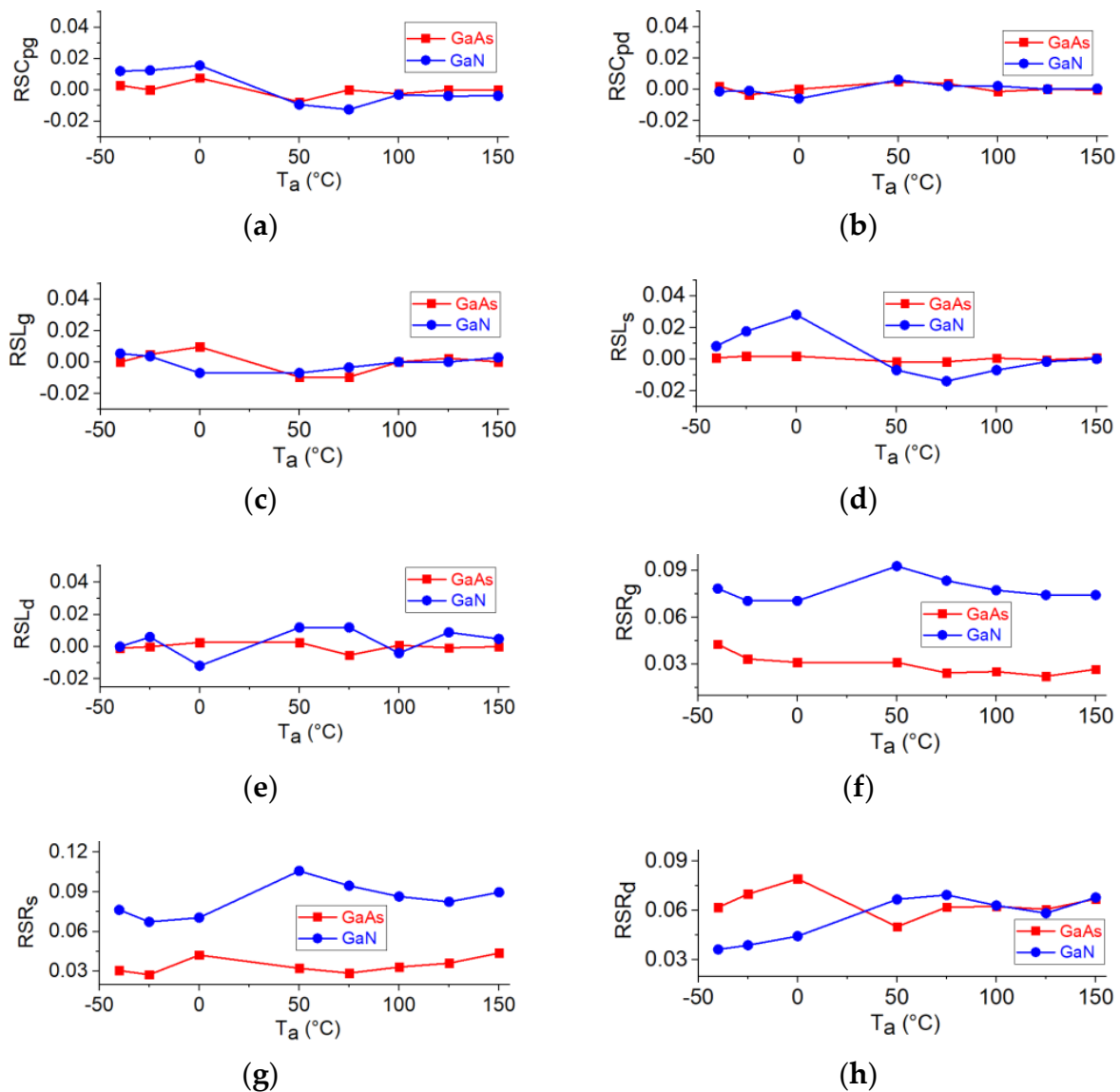

Figure 9. Behavior of the relative sensitivities of the extrinsic parameters versus T_a for the two studied devices.

Table 1. Parameters for GaAs and GaN HEMTs at 25 °C.

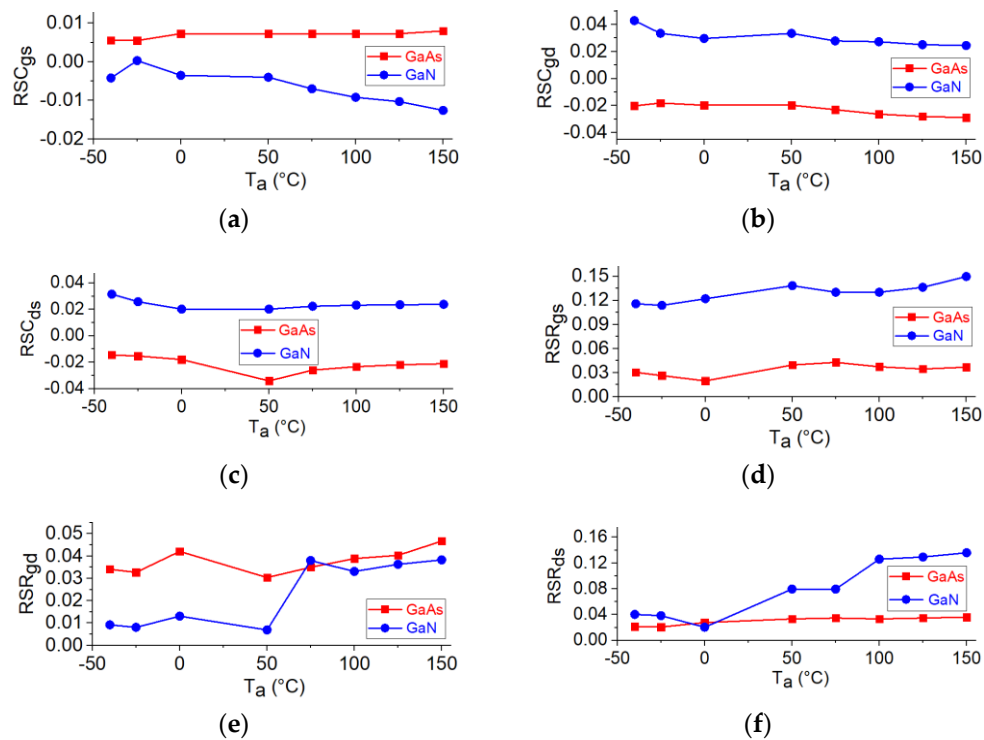| Parameters	GaAs HEMT	GaN HEMT
I_{ds} (mA)	14.7	63.5
C_{pg} (fF)	13.1	32.0
C_{pd} (fF)	41.6	50.0
L_g (pH)	104.0	142.0
L_s (pH)	5.41	1.43
L_d (pH)	37.8	84.0
R_g (Ω)	2.3	2.7
R_s (Ω)	4.0	3.1
R_d (Ω)	6.3	8.2
C_{gs} (fF)	275.0	199.9
C_{gd} (fF)	30.4	26.9
C_{ds} (fF)	55.9	89.2
R_{gs} (Ω)	1.5	1.2
R_{gd} (Ω)	6.3	13.0
R_{ds} (Ω)	360.0	322.4
g_m (mS)	29.6	63.0
τ_m (ps)	3.8	1.8
τ_{gs} (ps)	2.6	1.5
τ_{gd} (ps)	1.2	2.2
f_t (GHz)	14.9	40.0
f_{max} (GHz)	44.8	97.0

Figure 10. Behavior of the relative sensitivities of the intrinsic resistances and capacitances versus T_a for the two studied devices. The illustrated bias points are: V_{ds} = 3 V and V_{gs} = −0.1 V for the GaAs HEMT and V_{ds} = 9 V and V_{gs} = −4 V for the GaN HEMT.

Figure 11. Behavior of the relative sensitivities of the intrinsic transconductance, the intrinsic time constants, and the RF figures of merit versus T_a for the two studied devices. The illustrated bias points are: $V_{ds} = 3$ V and $V_{gs} = -0.1$ V for the GaAs HEMT and $V_{ds} = 9$ V and $V_{gs} = -4$ V for the GaN HEMT.
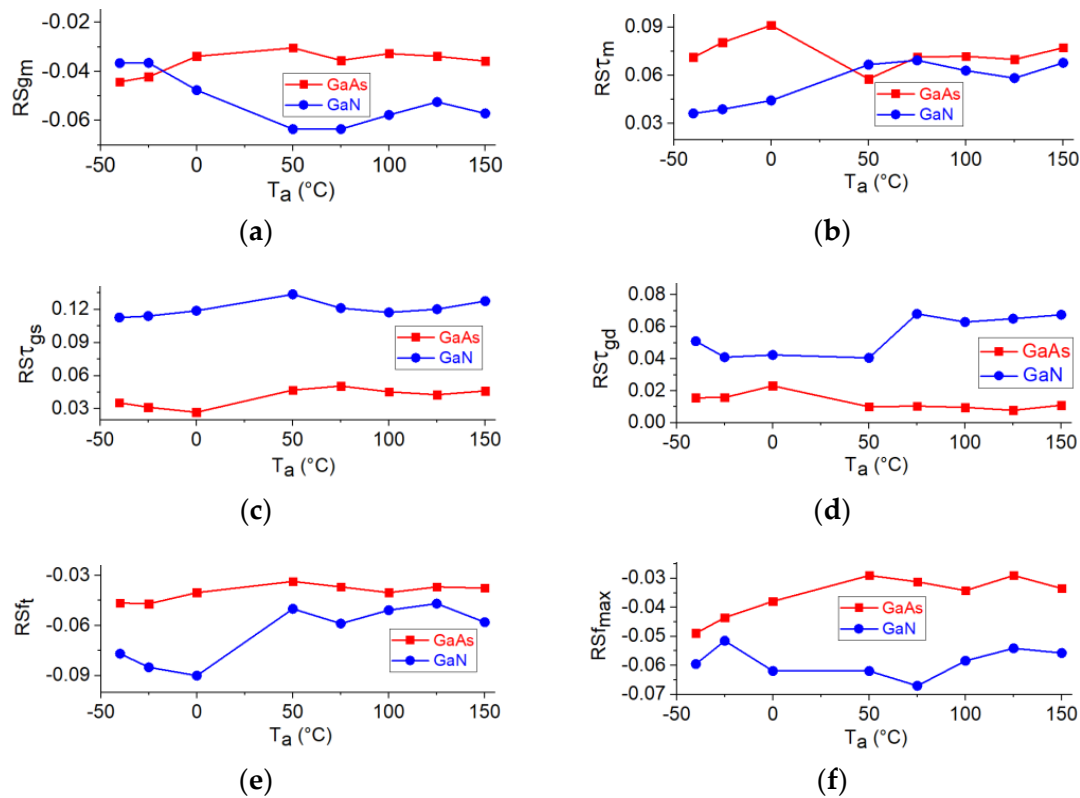
4. Conclusions

For the first time, an extensive and systematic comparative analysis of the GaAs and GaN HEMT technologies has been performed by investigating the impact of the temperature variations on the device performance in terms of the relative sensitivities of I_{ds}, ECPs, and major RF figures of merit over a broad temperature range, spanning from -40 °C to 150 °C. By increasing T_a, performance degradations are observed for both devices but they are more pronounced for the GaN technology. This can be attributed to the higher P_{diss} leading to a stronger degradation of the electron transport properties.

It is worth pointing out that establishing a fair comparison between the temperature-dependent performance of such inherently widely different semiconductor technologies is a very challenging task, since it is hard to define "homogeneous" operating conditions for devices exhibiting highly "heterogeneous" performances (e.g., the current density has to be referred to the tested technology) and to distinguish each contribution arising from the different peculiar features (e.g., different thermal conductivities of the substrates). In light of that, the selection of relatively balanced bias conditions has been based on the analysis of the specific DC output characteristics and then used as the benchmark for assessing the overall impact of T_a on the microwave characteristics of the two devices. The relative sensitivity has been chosen as an assessment indicator as this parameter allows one to evaluate quantitatively, systematically, and straightforwardly the impact of T_a on the microwave characteristics. Although the achieved findings are not of general validity as they can depend on the combined effects of ECPs whose values can change with the specific device, the investigation methodology is technology-independent and straightforwardly applicable to other FETs in order to target a quantitative and systematic comparison.

Author Contributions: Conceptualization, M.A.A. and G.C.; methodology, M.A.A. and G.C.; validation, M.A.A., A.Z.C. and S.I.; investigation, M.A.A., A.Z.C. and S.I.; writing—original draft

References

1. Mimura, T.; Hiyamizu, S.; Fujii, T.; Nanbu, K. A new field-effect transistor with selectively doped GaAs/n-AlxGa1-x as heterojunctions. *Jpn. J. Appl. Phys.* **1980**, *19*, L225–L227. [CrossRef]
2. Khan, M.A.; Bhattarai, A.; Kuznia, J.N.; Olson, D.T. High electron mobility transistor based on a GaN-AlxGa1-xN heterojunction. *Appl. Phys. Lett.* **1993**, *63*, 1214–1215. [CrossRef]
3. Belache, A.; Vanoverschelde, A.; Salmer, G.; Wolny, M. Experimental analysis of HEMT behavior under low-temperature conditions. *IEEE Trans. Electron Dev.* **1991**, *38*, 3–13. [CrossRef]
4. Anholt, R.E.; Swirhun, S.E. Experimental investigation of the temperature dependence of GaAs FET equivalent circuits. *IEEE Trans. Electron Dev.* **1992**, *39*, 2029–2036. [CrossRef]
5. Marinkovic, Z.; Markovic, V. Temperature-dependent models of low-noise microwave transistors based on neural networks. *Int. J. RF Microw. Comput. Aided Eng.* **2005**, *15*, 567–577. [CrossRef]
6. Caddemi, A.; Crupi, G.; Donato, N. On the soft breakdown phenomenon in AlGaAs/InGaAs HEMT: An experimental study down to cryogenic temperature. *Solid State Electron.* **2005**, *49*, 928–934. [CrossRef]
7. Caddemi, A.; Crupi, G.; Donato, N. Temperature effects on DC and small signal RF performance of AlGaAs/GaAs HEMTs. *Microelectron. Reliab.* **2006**, *46*, 169–173. [CrossRef]
8. Huang, J.C.; Hsu, W.C.; Lee, C.S.; Huang, D.H.; Huang, M.F. Temperature-dependent characteristics of enhancement-/depletion-mode double-doped AlGaAs/InGaAs pHEMTs and their monolithic DCFL integrations. *Solid State Electron.* **2007**, *51*, 882–887. [CrossRef]
9. Zhu, Y.; Karalkar, S.; Prasad, K.; Wei, C.; Mason, J.; Bartle, D. Temperature dependent linear HEMT model extracted with multi-temperature optimization. In Proceedings of the Asia Pacific Microwave Conference, Kaohsiung, Taiwan, 4–7 December 2012; pp. 756–759. [CrossRef]
10. Alim, M.A.; Rezazadeh, A.A. Temperature-dependent DC and small-signal analysis of AlGaAs/InGaAs pHEMT for high frequency applications. *IEEE Trans. Electron Dev.* **2016**, *63*, 1005–1012. [CrossRef]
11. Alim, M.A.; Rezazadeh, A.A. Device behaviour and zero temperature coefficients analysis for microwave GaAs HEMT. *Solid State Electron.* **2018**, *147*, 13–18. [CrossRef]
12. Alim, M.A.; Rezazadeh, A.A.; Crupi, G. Experimental insight into the temperature effects on DC and microwave characteristics for a GaAs pHEMT in multilayer 3-D MMIC technology. *Int. J. RF Microw. Comput. Aided Eng.* **2020**, *30*, e22379. [CrossRef]
13. Gryglewski, D.; Wojtasiak, W.; Kamińska, E.; Piotrowska, A. Characterization of self-heating process in GaN-based HEMTs. *Electronics* **2020**, *9*, 1305. [CrossRef]
14. Camarchia, V.; Cappelluti, F.; Pirola, M.; Guerrieri, S.D.; Ghione, G. Self-consistent electrothermal modeling of class A, AB, and B power GaN HEMTs under modulated RF excitation. *IEEE Trans. Microw. Theory Tech.* **2007**, *55*, 1824–1831. [CrossRef]
15. Darwish, A.M.; Huebschman, B.D.; Viveiros, E.; Hung, H.A. Dependence of GaN HEMT millimeter-wave performance on temperature. *IEEE Trans. Microw. Theory Tech.* **2009**, *57*, 3205–3211. [CrossRef]
16. Vitanov, S.; Palankovski, V.; Maroldt, S.; Quay, R. High-temperature modeling of AlGaN/GaN HEMTs. *Solid State Electron.* **2010**, *54*, 1105–1112. [CrossRef]
17. Crupi, G.; Avolio, G.; Raffo, A.; Barmuta, P.; Schreurs, D.M.M.-P.; Caddemi, A.; Vannini, G. Investigation on the thermal behavior for microwave GaN HEMTs. *Solid State Electron.* **2011**, *64*, 28–33. [CrossRef]
18. Angelotti, A.M.; Gibiino, G.P.; Florian, C.; Santarelli, A. Trapping dynamics in GaN HEMTs for millimeter-wave applications: Measurement-based characterization and technology comparison. *Electronics* **2021**, *10*, 137. [CrossRef]
19. Marinković, Z.; Crupi, G.; Caddemi, A.; Avolio, G.; Raffo, A.; Marković, V.; Vannini, G.; Schreurs, D.M.M.-P. Neural approach for temperature dependent modeling of GaN HEMTs. *Int. J. Numer. Model. Electron. Netw. Devices Fields* **2015**, *28*, 359–370. [CrossRef]
20. Crupi, G.; Raffo, A.; Avolio, G.; Schreurs, D.M.M.-P.; Vannini, G.; Caddemi, A. Temperature influence on GaN HEMT equivalent circuit. *IEEE Microw. Wirel. Comp. Lett.* **2016**, *26*, 813–815. [CrossRef]
21. Jarndal, A.; Ghannouchi, F.M. Improved modeling of GaN HEMTs for predicting thermal and trapping-induced-kink effects. *Solid-State Electron.* **2016**, *123*, 19–25. [CrossRef]
22. Alim, M.A.; Rezazadeh, A.A.; Gaquiere, C. Temperature effect on DC and equivalent circuit parameters of 0.15-μm gate length GaN/SiC HEMT for microwave applications. *IEEE Trans. Microw. Theory Tech.* **2016**, *64*, 3483–3491. [CrossRef]
23. Rodríguez, R.; González, B.; García, J.; Núñez, A. Electrothermal DC characterization of GaN on Si MOS-HEMTs. *Solid-State Electron.* **2017**, *137*, 44–51. [CrossRef]
24. Jarndal, A. Neural network electrothermal modeling approach for microwave active devices. *Int. J. RF Microw. Comput. Aided Eng.* **2019**, *29*, e21764. [CrossRef]

25. Crupi, G.; Raffo, A.; Vadalà, V.; Vannini, G.; Caddemi, A. High-periphery GaN HEMT modeling up to 65 GHz and 200 °C. *Solid-State Electron.* **2019**, *152*, 11–16. [CrossRef]

26. Chen, Y.; Xu, Y.; Zhou, J.; Kong, Y.; Chen, T.; Zhang, Y.; Yan, B.; Xu, R. Temperature-dependent small signal performance of GaN-on-diamond HEMTs. *Int. J. Numer. Model. Electron. Netw. Devices. Field* **2020**, *33*, e2620. [CrossRef]

27. Majumdar, A.; Chatterjee, S.; Chatterjee, S.; Chaudhari, S.S.; Poddar, D.R. An ambient temperature dependent small signal model of GaN HEMT using method of curve fitting. *Int. J. RF Microw. Comput. Aided Eng.* **2020**, *30*, e22434. [CrossRef]

28. Giofré, R.; Colantonio, P.; Gonzalez, L.; De Arriba, F.; Cabria, L.; Molina, D.L.; Garrido, E.C.; Vitobello, F. Design realization and tests of a space-borne GaN solid state power amplifier for second generation Galileo navigation system. *IEEE Trans. Aerosp. Electron. Syst.* **2018**, *54*, 2383–2396. [CrossRef]

29. Darwish, A.M.; Bayba, A.J.; Hung, H.A. Accurate determination of thermal resistance of FETs. *IEEE Trans. Microw. Theory Tech.* **2005**, *53*, 306–313. [CrossRef]

30. Sarua, A.; Ji, H.; Hilton, K.P.; Wallis, D.J.; Uren, M.J.; Martin, T.; Kuball, M. Thermal boundary resistance between GaN and substrate in AlGaN/GaN electronic devices. *IEEE Tran. Electron Dev.* **2007**, *54*, 3152–3158. [CrossRef]

31. Kuzmík, J.; Bychikhin, S.; Pogany, D.; Gaquière, C.; Pichonat, E.; Morvan, E. Investigation of the thermal boundary resistance at the III-nitride/substrate interface using optical methods. *J. Appl. Phys.* **2007**, *101*, 054508-1–054508-6. [CrossRef]

32. Florian, C.; Santarelli, A.; Cignani, R.; Filicori, F. Characterization of the nonlinear thermal resistance and pulsed thermal dynamic behavior of AlGaN–GaN HEMTs on SiC. *IEEE Trans. Microw. Theory Tech.* **2013**, *61*, 1879–1891. [CrossRef]

33. Coutu, R.; Lake, R.; Christiansen, B.; Heller, E.; Bozada, C.; Poling, B.; Via, G.; Theimer, J.; Tetlak, S.; Vetury, R.; et al. Benefits of considering more than temperature acceleration for GaN HEMT life testing. *Electronics* **2016**, *5*, 32. [CrossRef]

34. Zheng, Q.; Li, C.; Rai, A.; Leach, J.H.; Broido, D.A.; Cahill, D.G. Thermal conductivity of GaN, ^{71}GaN, and SiC from 150 K to 850 K. *Phys. Rev. Mater.* **2019**, *3*, 014601. [CrossRef]

35. Jang, K.-W.; Hwang, I.-T.; Kim, H.-J.; Lee, S.-H.; Lim, J.-W.; Kim, H.-S. Thermal analysis and operational characteristics of an AlGaN/GaN high electron mobility transistor with copper-filled structures: A simulation study. *Micromachines* **2019**, *11*, 53. [CrossRef] [PubMed]

36. Mitterhuber, L.; Hammer, R.; Dengg, T.; Spitaler, J. Thermal characterization and modelling of AlGaN-GaN multilayer structures for HEMT applications. *Energies* **2020**, *13*, 2363. [CrossRef]

37. Walters, P.; Pollard, R.; Richardson, J.; Gamand, P.; Suchet, P. On-wafer measurement uncertainty for 3-terminal active millimetre-wave devices. In Proceedings of the GaAs IC Symposium Technical Digest 1992, Miami Beach, FL, USA, 4–7 October 1992; pp. 55–58.

38. Lewandowski, A.; Williams, D.F.; Hale, P.D.; Wang, J.C.M.; Dienstfrey, A. Covariance-based vector-network-analyzer uncertainty analysis for time-and frequency-domain measurements. *IEEE Trans. Microw. Theory Tech.* **2010**, *58*, 1877–1886. [CrossRef]

39. Garelli, M.; Ferrero, A. A unified theory for S-parameter uncertainty evaluation. *IEEE Trans. Microw. Theory Tech.* **2012**, *60*, 3844–3855. [CrossRef]

40. King, F.D.; Winson, P.; Snider, A.D.; Dunleavy, L.; Levinson, D.P. Math methods in transistor modeling: Condition numbers for parameter extraction. *IEEE Trans. Microw. Theory Tech.* **1998**, *46*, 1313–1314. [CrossRef]

41. Fager, C.; Linner, L.J.P.; Pedro, J.C. Optimal parameter extraction and uncertainty estimation in intrinsic FET small-signal models. *IEEE Trans. Microw. Theory Tech.* **2002**, *50*, 2797–2803. [CrossRef]

42. Luo, D.; Shen, L.; Gao, J. An improved linear modeling technique with sensitivity analysis for GaN HEMT. *Int. J. Numer. Model. Electron. Netw. Devices Fields* **2017**, *30*, e2139. [CrossRef]

43. Cao, K.-J.; Zhang, A.; Gao, J. Sensitivity analysis and uncertainty estimation in small-signal modeling for InP HBT (invited paper). *Int. J. Numer. Model. Electron. Netw. Devices Fields* **2021**, 1–11. [CrossRef]

44. Lu, S.-S.; Chen, T.-W.; Chen, H.-C.; Meng, C. The origin of the kink phenomenon of transistor scattering parameter S22. *IEEE Trans. Microw. Theory Tech.* **2001**, *49*, 333–340. [CrossRef]

45. Crupi, G.; Raffo, A.; Caddemi, A.; Vannini, G. The kink phenomenon in the transistor S22: A systematic and numerical approach. *IEEE Microw. Wirel. Comp. Lett.* **2012**, *22*, 406–408. [CrossRef]

46. Crupi, G.; Raffo, A.; Marinkovic, Z.; Avolio, G.; Caddemi, A.; Markovic, V.; Vannini, G.; Schreurs, D.M.M.-P. An extensive experimental analysis of the kink effects in S22 and h21 for a GaN HEMT. *IEEE Trans. Microw. Theory Tech.* **2014**, *62*, 513–520. [CrossRef]

47. Ahsan, S.A.; Ghosh, S.; Khandelwal, S.; Chauhan, Y.S. Modeling of kink-effect in RF behaviour of GaN HEMTs using ASM-HEMT model. In Proceedings of the IEEE International Conference Electron Devices Solid-State Circuits, Hong Kong, China, 3–5 August 2016; pp. 426–429. [CrossRef]

48. Alim, M.A.; Rezazadeh, A.A.; Gaquiere, C.; Crupi, G. Thermal influence on S22 kink behavior of a 0.15-μm gate length AlGaN/GaN/SiC HEMT for microwave applications. *Semicond. Sci. Tech.* **2019**, *34*, 1–8. [CrossRef]

49. Crupi, G.; Raffo, A.; Vadalà, V.; Vannini, G.; Caddemi, A. A new study on the temperature and bias dependence of the kink effects in S22 and h21 for the GaN HEMT Technology. *Electronics* **2018**, *7*, 353. [CrossRef]

50. Crupi, G.; Caddemi, A.; Schreurs, D.M.M.-P.; Dambrine, G. The large world of FET small-signal equivalent circuits. *Int. J. RF Microw. Comput. Aided Eng.* **2016**, *26*, 749–762. [CrossRef]

51. Crupi, G.; Schreurs, D.M.M.-P.; Caddemi, A.; Raffo, A.; Vannini, G. Investigation on the non-quasi-static effect implementation for millimeter-wave FET models. *Int. J. RF Microw. Comput. Aided Eng.* **2010**, *20*, 87–93. [CrossRef]